AUGUST 09 2023

A neural network-based method for spruce tonewood characterization

David Giuseppe Badiane; Sebastian Gonzalez; Raffaele Malvermi ; Fabio Antonacci ; Augusto Sarti

J. Acoust. Soc. Am. 154, 730–738 (2023)
https://doi.org/10.1121/10.0020559

JASA ARTICLE

A neural network-based method for spruce tonewood characterization

David Giuseppe Badiane, Sebastian Gonzalez, Raffaele Malvermi,[a] Fabio Antonacci, and Augusto Sarti
Department of Electronics, Information and Bioengineering, Politecnico di Milano, Milan, Italy

ABSTRACT:
The acoustical properties of wood are primarily a function of its elastic properties. Numerical and analytical methods for wood material characterization are available, although they are either computationally demanding or not always valid. Therefore, an affordable and practical method with sufficient accuracy is missing. In this article, we present a neural network-based method to estimate the elastic properties of spruce thin plates. The method works by encoding information of both the eigenfrequencies and eigenmodes of the system and using a neural network to find the best possible material parameters that reproduce the frequency response function. Our results show that data-driven techniques can speed up classic finite element model updating by several orders of magnitude and work as a proof of concept for a general neural network-based tool for the workshop.
 https://doi.org/10.1121/10.0020559
(Received 12 December 2022; revised 14 July 2023; accepted 17 July 2023; published online 9 August 2023)
[Editor: Andrew Morrison] Pages: 730–738

I. INTRODUCTION

Wood selection is one of the most important issues in stringed instrument making: Wood displays a high intra-species, inter-species, intra-specimen, and inter-specimen variability in its material properties (Wegst, 2006), yet those very same material properties play a crucial role in the design of the instrument (Yoshikawa, 2007). Typically, luthiers focus on the density and the longitudinal Young's modulus of the instrument soundboard (Barlow, 1997). However, several elastic constants contribute to the acoustics of the soundboard, in particular, the radial Young's modulus and the longitudinal to radial shear modulus (Obataya *et al.*, 2000; Viala *et al.*, 2020). Moreover, multiple components of a stringed instrument—including the strings and their supporting area—have a primary impact on the instrument vibrational properties. Indeed, recent studies on a classical guitar (Brauchler *et al.*, 2022a; Brauchler *et al.*, 2022b) show that the material properties of the guitar back-plate, neck, and bracing are highly correlated to the eigenfrequencies of the complete instrument. Accurately measuring those constants is of paramount importance when consistency of production is required.

In this context, luthiers often fail in the selection of wood with the best acoustical performance (Ball, 2007; Buksnowitz *et al.*, 2007). Indeed, few makers employ a scientific approach to select wood (Carlier *et al.*, 2018). Nonetheless, the scientific community has developed numerous vibrational non-destructive (ND) techniques to identify the material properties of wood. Focusing only on the most popular ones, we can name ultrasonic wave propagation (Fang *et al.*, 2017), Lamb wave propagation (Lasn *et al.*, 2011), and finite element model (FEM) updating methods (Farhat and Hemez, 1993).

Among these, FEM updating has been widely and successfully applied to characterize wooden bodies with arbitrary geometry (Larsson, 1997; Viala *et al.*, 2018; Zhou *et al.*, 2017). In practice, these methods perform the identification of the material parameters through the minimization of a cost function. Typically, the cost function is the relative difference between a prescribed number of eigenfrequencies of the body under analysis and their predictions obtained from a finite element simulation. An in-depth description of FEM updating can be found in Mottershead *et al.* (2011).

However, FEM updating approaches are not widely employed by instrument makers since they may require advanced measuring techniques, e.g., a laser vibrometer as in Brauchler *et al.* (2021) and Viala *et al.* (2018), or multiple measurements, as in Araújo *et al.* (1996) and Sol *et al.* (1993), if the modal information is to be retrieved, making them very time-consuming. Furthermore, since they are usually based on complex numerical models, these methods are computationally expensive and are beyond the technical abilities of the average luthier.

One way to speed up FEM updating methods is to employ machine learning techniques (Bock *et al.*, 2019). Indeed, neural networks (NNs) can be used in place of a FEM simulation to obtain the eigenfrequencies of a body in a computational time that can be down to 1/1000th of the time required by FEM without a significant sacrifice of accuracy (Badiane *et al.*, 2022; Gonzalez *et al.*, 2021; Salvi *et al.*, 2021). However, NN-based methods for the characterization of tonewood are still missing.

It is important to mention that a fast state-of-the-art method for tonewood characterization is already available in instrument making, although applicable only to rectangular

[a]Electronic mail: raffaele.malvermi@polimi.it

https://doi.org/10.1121/10.0020559

wooden plates. Indeed, Caldersmith (1984); McIntyre and Woodhouse (1988), and McIntyre and Woodhouse (1986) introduce a set of equations to estimate the most important elastic constants of a wooden plate starting from a subset of its eigenfrequencies. However, the validity and the accuracy of such formulas vary with the plate geometry and can thus lead to non-negligible errors when using non-rectangular plates, as one usually finds in guitar-making.

In this article, we present a novel NN-based technique to identify the elastic constants of a thin rectangular spruce plate with given dimensions and density. The technique is called *FRF2Params*, as it requires the measurement of a single frequency response function (FRF) (Fletcher and Rossing, 2012) to estimate the plate material parameters (Params). *FRF2Params* is based on the minimization of a cost function that takes into account both the frequency and the amplitude of the peaks of the measured and modeled FRFs, predicted at each minimization step by two NNs, one for the frequency and another for the amplitude. In this way, by learning the behavior of the amplitude, the NN is actually learning about the modal shapes present in the top plate, information that up until now has not been included in the material characterization.

Since NNs approximate the relation between material parameters and eigenfrequencies through a set of non-linear equations, *FRF2Params* represents a middle ground between full-fledged FEM updating methods and the analytical formulas mentioned above. In particular, *FRF2Params* is both fast and robust to modifications of the plate geometry. If properly trained, in fact, NNs can be used to model arbitrary geometries (Gonzalez *et al.*, 2021), making this method easily extendable to other objects.

The paper is organised as follows: in Sec. II, the problem of the identification of the plate material properties from a single FRF is presented. In Sec. III, an in-depth description of the *FRF2Params* method is provided. In Sec. IV, the generation of the dataset used to train the NNs is illustrated. In Sec. V, the prediction accuracy of the NNs is discussed, and *FRF2Params* is applied to characterize a set of ten thin plates of Norway spruce (*Picea abies*).

II. PROBLEM FORMULATION

To build the soundboard of a classical guitar, guitar makers start from two thin rectangular plates of wood, often spruce. The plates are glued together as shown in Fig. 1(a). The geometry of each plate is characterized by its length l, width w, and thickness h. Although the size of the plate depends on the supplier and the guitar model to be built, reasonable nominal dimensions are $(580 \times 220 \times 4)$ mm in the (L, R, T) reference system, where L, R, and T correspond to the wood grain direction (longitudinal), the direction normal to the growth rings (radial), and the direction tangential to the growth rings (tangential), respectively. The employed reference system is reported at the bottom of Fig. 1(a). We will refer to such plates as *classical guitar plates*.

We model the elastic behavior of wood in the (L, R, T) reference system by assuming a linear elastic and homogeneous material. In particular, a simplified orthotropic model is employed, such that nine elastic constants, namely three Young's moduli (E_L, E_R, E_T), three shear moduli (G_{LR}, G_{RT}, G_{LT}), and three Poisson's ratios $(\nu_{LR}, \nu_{RT}, \nu_{LT})$ completely characterize the material (Ross, 2010). We will denote them as *material parameters*. Typically, it is assumed that vibration does not occur along the tangential direction when considering thin plates. Therefore, only the parameters $(E_L, E_R, G_{LR}, \nu_{LR})$ are normally considered as relevant to model the plate material. We decided to employ

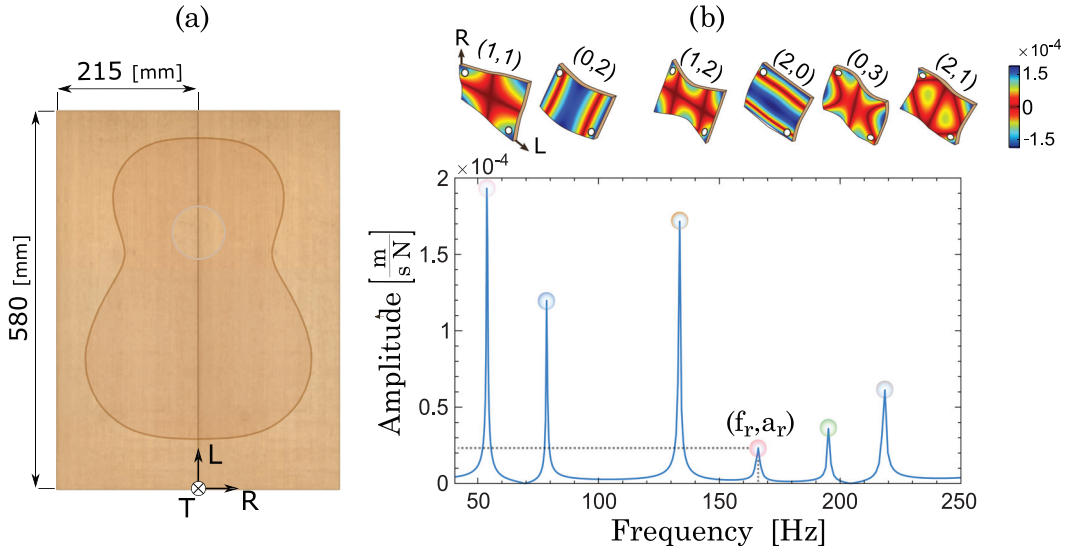

FIG. 1. (Color online) (a) Diagram of two classical guitar plates glued together. Although the plate geometry depends on the supplier, reasonable nominal dimensions are $(580 \times 220 \times 4)$ mm according to the (L, R, T) reference system reported at the bottom of the figure. (b) Simulated FRF and modal shapes of a classical guitar plate with standard geometry, nominal elastic constants shown in Table I, and density $\rho = 421\,\mathrm{kgm}^{-3}$. The FRF is evaluated in terms of a mobility, i.e., the ratio between plate velocity and exerted force. The measurement points at which the FRF is evaluated are placed at 20 mm from the edges of the bottom-left and top-right corners of the plate and are denoted with white disks over the modal shapes.

TABLE I. Center values of the material parameters in the dataset, i.e., nominal elastic constants of Norway spruce (*P. abies*) (Hearmon, 1948).

$E_{L_0} = 10.9\,\text{GPa}$	$G_{LR_0} = 580\,\text{MPa}$	$\nu_{LR} = 0.39$
$E_{R_0} = 640\,\text{MPa}$	$G_{RT_0} = 26\,\text{MPa}$	$\nu_{RT} = 0.64$
$E_{T_0} = 420\,\text{MPa}$	$G_{LT_0} = 590\,\text{MPa}$	$\nu_{LT} = 0.49$

here the complete orthotropic model, since we are interested in a general method that can be applied also to different geometries.

Our aim is to estimate the material parameters of a classical guitar plate from a single mobility FRF, that is, the ratio between the plate velocity and the force applied to it, evaluated at a pair of prescribed measurement points. Figure 1(b) shows an example FRF, measured at 20 mm from the edges of the bottom-left and top-right corners of a "virtual" plate. The virtual plate, modeled with the finite element method, has nominal dimensions, the material parameters shown in Table I, and density $\rho = 421\,\text{kg m}^{-3}$. The FRF amplitude, reported in linear scale, is characterized by a sequence of R peaks in the low-frequency range. We denote each peak with its frequency location and amplitude value, i.e., $(\hat{f}_r, \hat{a}_r)$ with $r = 1, \ldots, R$. The FRF is measured as a mobility in a 2 mm radius circular area at the impact point of the hammer.

It must be noted that the set of identifiable peaks inside the FRF corresponds to a subset of the plate modes within the same frequency range (Meirovitch, 2001). The plate modes, in fact, are characterized by an eigenfrequency f_s, a modal damping ratio ξ_s (Fletcher and Rossing, 2012), with $s = 1, \ldots, S$ and $S \geq R$, and a modal shape, i.e., the normal velocity field when the plate surface vibrates at f_s. The FRF amplitude a_s evaluated at f_s can be approximated as a function of the three modal features (Malvermi *et al.*, 2022). The selected measurement points can be at the nodal lines (i.e., regions of zero velocity) of a mode. In this case, a_s will correspond to a local minimum of the FRF instead of a peak.

The inset in Fig. 1(b) shows the modal shapes of the virtual plate that are excited at the chosen measurement points. The measurement points are denoted with white disks over each modal shape. The nodal lines and the maxima inside the modal shape are highlighted in dark red and blue, respectively. Each modal shape is labelled using the notation based on nodal lines presented in Fletcher and Rossing (2012).

Given a classical guitar plate, the values of f_s and a_s associated with the sth low-frequency mode are related to the material, geometric, and damping properties of the plate by means of two continuous functionals $\mathcal{F}_s$ and $\mathcal{A}_s$, namely,

$$f_s \approx \mathcal{F}_s(M_1, \ldots, M_9, \rho, l, w, h, \xi_s), \tag{1}$$

$$a_s \approx \mathcal{A}_s(M_1, \ldots, M_9, \rho, l, w, h, \xi_s), \tag{2}$$

where M_k with $k = 1, \ldots, 9$ are the material parameters of the plate. Therefore, the identification of the plate material parameters starting from a measured FRF can be formulated as the inversion of Eqs. (1) and (2) with respect to M_k, given the pair $(\hat{f}_r, \hat{a}_r)$ as part of the inputs of the inverse problem. However, the different nature of the modes within the FRF, which may be either peaks or local minima, makes Eq. (2) highly non-linear and, thus, not easily invertible. For this reason, we regress the two functionals by means of NNs trained with the outcomes of a FEM.

III. METHODOLOGY

FRF2Params takes as input the peaks of one measured FRF $(\hat{f}_r, \hat{a}_r)$, the plate density ρ, and the plate dimensions (l, w, h). The updating stage of the method is based on the minimization of a cost function between $(\hat{f}_r, \hat{a}_r)$ and the eigenfrequency and FRF amplitude of the corresponding plate mode, i.e., (f_s, a_s), predicted by the NNs. The minimization is achieved with the MATLAB® function FMINSEARCH, which applies the Nelder–Mead simplex direct search algorithm (Lagarias *et al.*, 1998), as it does not need to compute gradients, and it guarantees stability also with discontinuous cost functions as in our case.

The updating is limited only to the plate material parameters. Figure 2 shows the pipeline of the parameter updating procedure. The NNs predict the pairs (f_s, a_s), with $s = 1, \ldots, S$, associated with the plate modes. The predictions of the NNs are employed along with the peaks of the FRF to compute the cost function. The material parameters are iteratively updated to minimize the cost function until the termination criteria are met.

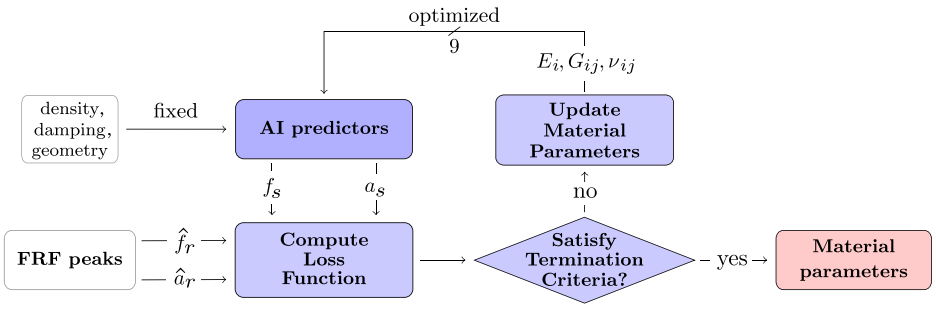

FIG. 2. (Color online) Flow chart of the minimization procedure within the *FRF2Params* method. Only the material parameters of the plate are subject to update. Once fed with the inputs, the neural networks predict the pairs (f_s, a_s) associated with the plate modes. The cost function in Eq. (7) is computed in the frequency/amplitude space. The material parameters are updated at each minimization step until the termination criteria of the minimization procedure are met.

https://doi.org/10.1121/10.0020559

The minimization procedure starts from a first guess of the plate material parameters, i.e., the elastic constants reported in Table I. To enhance the robustness of the solution, we use as final estimate the average over the outputs of ten runs of the minimization procedure. At each run, the density is sampled from a Gaussian random variable with the measured plate density as mean and a standard deviation equal to the 2.5% of the center value, thus, modeling the error associated with the measurement of the density. We do this to account for the variability in the height of the plate, as it is the largest uncertainty in our measurements. A single minimization run takes approximately 40 s on a laptop.

A. Cost function computation and model updating

The cost function for the optimisation is defined in the frequency/amplitude space. Both $(\hat{f}_r, \hat{a}_r)$ and (f_s, a_s) can be represented as points of this space. In particular, a mode matching operation is performed to discard the eigenfrequencies corresponding to local minima inside the FRF. We do so by computing the relative difference between the frequency $\hat{f}_r$ of each FRF peak and the *nearest* plate eigenfrequency f_s in the frequency/amplitude space. The amplitude information is used only in the mode matching stage. This last part is fundamental as it implicitly takes into account the amplitude in a cost function that only depends on the eigenfrequencies.

Let us consider the two sets of pairs characterizing the experimental FRF peaks and the predicted plate modes, namely, $\{(\hat{f}_r, \hat{a}_r)\}_{r=1,\dots,R}$ and $\{(f_s, a_s)\}_{s=1,\dots,S}$, respectively, where $R = 12$ and $S = 15$. Both the experimental FRF amplitudes $\hat{a}_r$ and their numerical counterparts a_s are expressed in dB scale. As the amplitudes of the experimental FRF peaks are not obtained in "ideal" conditions due to both the hammer and the impact characteristics (Mali and Singru, 2018), we normalize the simulated amplitudes through

$$a_s^* = a_s + 20\,\log_{10}\left(\frac{1}{K}\sum_{k=1}^{K}\frac{\hat{a}_k|_{\text{lin}}}{a_k|_{\text{lin}}}\right), \tag{3}$$

where a_s^* is the normalized amplitude associated with f_s and is expressed in dB, $K = 5$ to take into account the first peaks according to Mali and Singru (2018), $\hat{a}_k|_{\text{lin}}$ and $a_k|_{\text{lin}}$ are the amplitudes $\hat{a}_r$ and a_s in linear scale, respectively, and $r = s = k$, respectively.

We compute the matrix $\mathrm{D} \in \mathbb{R}^{R\times S}$ of the Euclidean distances between all the combinations of $(\hat{f}_r, \hat{a}_r)$ and (f_s, a_s^*). A single entry of this matrix is calculated as

$$[\mathrm{D}]_{r,s} = \sqrt{(\hat{f}_r - f_s)^2 + \left[\eta(\hat{a}_r - a_s^*)\right]^2}, \tag{4}$$

where the coefficient

$$\eta = \frac{1}{R}\sum_{r=1}^{R}\frac{\hat{f}_r}{\hat{a}_r} \tag{5}$$

is used to give the same weight to frequencies and amplitudes in the computation of the distance.

Therefore, for each $\hat{f}_{\bar{r}}$ with $\bar{r} = 1, \dots, R$ we can detect the index of the *nearest* f_s as

$$[\chi]_{\bar{r}} = \text{argmin}_s\{[\mathrm{D}]_{r,s} \,|\, r = \bar{r} \wedge s = 1, \dots, S\}, \tag{6}$$

such that $\boldsymbol{\chi} \in \mathbb{R}^{R\times 1}$.

Finally, the cost function $\hat{L}_2$ is computed as

$$\hat{L}_2 = \sum_{r=1}^{R} w_r \left(\frac{\hat{f}_r - f_{[\chi]_r}}{\hat{f}_r}\right)^2 + J_\chi, \tag{7}$$

$$w_r = \begin{cases} 1.2 & \text{if} \quad r \le 5 \\ 1 & \text{otherwise}, \end{cases} \tag{8}$$

$$J_\chi = (R - A)^2, \tag{9}$$

where (i) w_r is the rth entry of a vector of weights $\mathbf{w}$ and allows us to slightly prioritize the frequency matching between lower frequency modes, as they are more correlated to the plate material properties as shown in Caldersmith (1984); (ii) $f_{[\chi]_r}$ is the *nearest* f_s with respect to $\hat{f}_r$; (iii) A is the number of distinct values belonging to χ (i.e., the cardinality of χ), and J_χ is a penalty function to avoid the condition in which two or more $\hat{f}_r$ are associated with the same f_s (note that when this condition occurs, $R > A$ and $J_\chi > 0$).

B. FRF measurements

For the experimental results, a dynamometric hammer with light tip (086E80, PCB Piezotronics, Depew, NY) and a uniaxial accelerometer (352A12, PCB Piezotronics) were used to generate an impulsive excitation and measure the harmonic response, respectively. For each measurement, six time-domain signals of 2 s sampled at 48 kHz were acquired. FRFs were then estimated following the definition of the H1 estimator to reduce noise caused by the instrumentation (Schwarz and Richardson, 1999). The magnitudes of the resulting FRFs are represented in dB scale, with a reference value equal to $1\,\text{ms}^{-1}\,\text{N}^{-1}$. The mass of the accelerometer is not considered in the FEM simulations for the sake of simplicity.

IV. DATASET GENERATION

We model the classical guitar plate with a FEM of a thin rectangular plate with orthotropic material on *COMSOL Multiphysics*®. In our application, the measurement points of the FRF are located 20 mm from the edges of the bottom-left and top-right corners of the plate, and the impulsive force has a constant spectrum. The measurement points are located near the plate corners to excite more modes, as indicated in Mali and Singru (2018).

We randomly sample Eqs. (1) and (2) by computing the eigenfrequency f_s and the amplitude a_s associated with the first $S = 15$ plate modes with an *Eigenfrequency study* and a

Frequency domain study, respectively. The plate material parameters and geometry are sampled by means of 13 independent Gaussian random variables as follows:

$$Y = Y_0(1 + \delta_Y), \tag{10}$$

where Y is the sampled property, Y_0 is its center value, and δ_Y is a zero-mean Gaussian random variable.

The center values of the material parameters correspond to the nominal values of Norway spruce (Hearmon, 1948) reported in Table I. The center values of the density and the geometric parameters are set to $\rho_0 = 421\,\text{kg m}^{-3}$ and $(l_0 \times w_0 \times h_0) = (580 \times 220 \times 4)\,\text{mm}$, respectively. The standard deviation of the Gaussian random variables δ_Y is $\sigma_M = 0.3$ for the material parameters, $\sigma_\rho = 0.1$ for the density, $[\sigma_l, \sigma_w, \sigma_h] = [0.01, 0.03, 0.075]$ for the geometric parameters.

We employ the Rayleigh damping model (Rayleigh, 2013) and randomly sample its two control parameters α and β as

$$\alpha = \alpha_0(1 + U(-1,1)) \quad [\text{s}^{-1}], \tag{11}$$

$$\beta = 2 \times 10^{U(-1,1)-6} \quad [\text{s}], \tag{12}$$

where $U(-1,1)$ is a uniform random variable ranging within $[-1,1]$, and $\alpha_0 = 50\,\text{s}^{-1}$. We sample Eqs. (1) and (2) 4500 times, thus, obtaining a dataset of 4500 occurrences with 15 inputs (i.e., nine elastic constants, three geometric parameters, two damping parameters, and density) and 30 outputs (f_s, a_s) with $s = 1, \ldots, 15$. This dataset is used to train the NNs.

Figure 3 shows the correlation matrix between the mechanical parameters and the frequency and amplitude of the simulated FRF obtained in the dataset. Despite only a few parameters being correlated to the features of the FRF, we will optimise for all of them as we do not want to force the optimisation algorithm to select a path during the optimisation. Small variation in the irrelevant parameters, in fact, can help the minimization to search more efficiently the parameter space. Note how the damping parameters are especially relevant for the amplitude of the FRF and how the thickness variation has the same qualitative behavior as the density variation for the frequencies. It is because of this that in our optimisation procedure we only vary the material parameters and leave the geometric parameters at nominal values: Variations in the thickness enter into the algorithm through uncertainty in the density of the plate.

V. RESULTS

A. Prediction accuracy of the NNs

We employ two multi-layer feedforward neural networks (MFNNs) (Svozil *et al.*, 1997) to predict f_s and a_s as they are reckoned to be universal approximators of general mappings from one finite dimensional space to another (Hornik *et al.*, 1989). In this work, the MATLAB® machine learning toolbox NNTRAINTOOL (Aldakheel *et al.*, 2021; Beale *et al.*, 1992) is used to implement and train the MFNNs following the Levenberg–Marquardt algorithm (Moré, 1978). To train and test the NNs, we randomly split the dataset presented in Sec. IV into train and test sets containing 90% and 10% of the total occurrences, respectively.

The quality of the estimation provided by the MFNNs is assessed by evaluating the average coefficient of determination $\overline{R^2}$, defined as

$$\overline{R^2} = \frac{1}{S}\sum_{s=1}^{S} R_s^2, \quad s = 1, \ldots, S, \tag{13}$$

where $S = 15$, and R_s^2 is the coefficient of determination (Glantz and Slinker, 2001) related to the estimation of the sth output in the test set.

The total number of layers $\mathcal{L}$ and the number of neurons per layer $\mathcal{M}$ define the topology of the MFNN, indicated as $(\mathcal{M} \times \mathcal{L})$. The accuracy of the MFNN can be enhanced by optimising its topology, so that the expressivity of the network meets the complexity of the training data. This optimisation stage is commonly referred to as hyperparameters tuning.

Concerning the estimation of the frequencies, we follow the same rationale as Gonzalez *et al.* (2021), where a (7×1) NN was employed to correctly predict the first five eigenfrequencies of a violin top plate. We employ a (17×1) NN, with 17 being the number of predicted

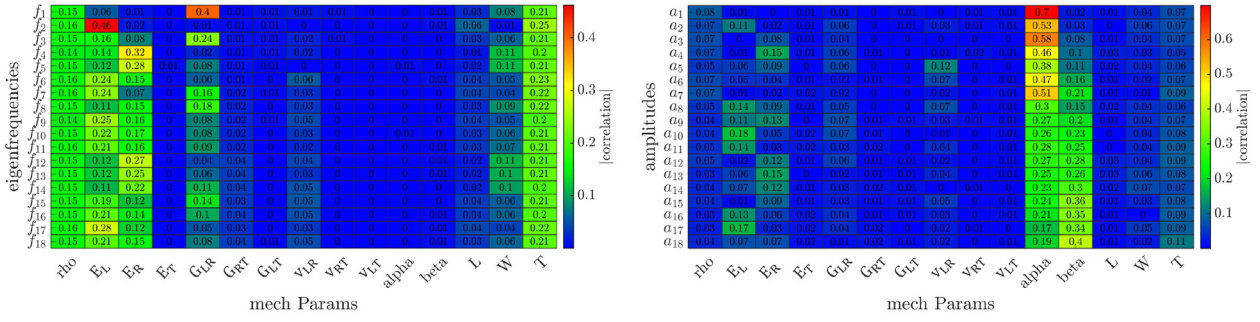

FIG. 3. (Color online) Correlation matrix between the mechanical parameters and the frequencies and amplitudes of the simulated FRF. The correlation coefficients are computed in all the dataset for the given spread in each parameter. Note how the damping parameters are extremely relevant for the amplitude of the FRF yet not for the frequency. Moreover, it can be noted that the thickness variation has the same qualitative behavior as the density variation, thus, having the same relevance for the frequency.

https://doi.org/10.1121/10.0020559

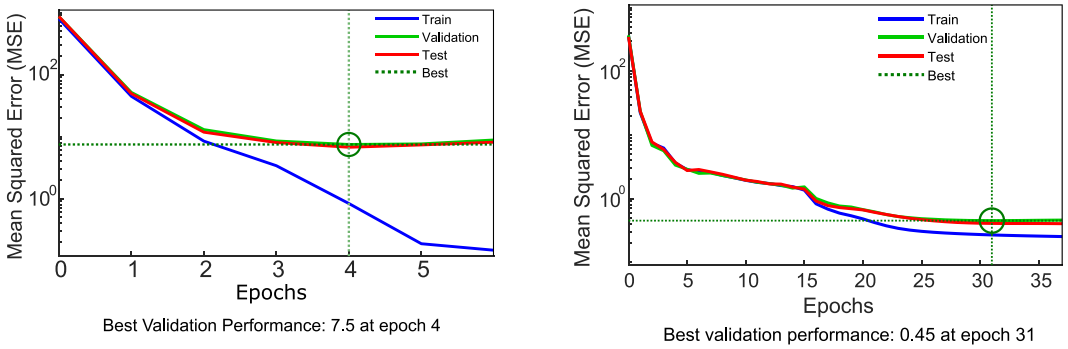

FIG. 4. (Color online) (Left) Train, test, and validation losses versus the epoch number for a (64×4) MFNN. The model is too complex for the training data. As a result, overfitting is not avoided, and the mean squared error on the validation set, i.e., the best validation performance, is high. (Right) Train, test, and validation losses versus the epoch number for a (24×2) MFNN. The expressivity of the model meets the complexity of the training data. Therefore, the discrepancy between the losses stays acceptable until the plateau is reached and the early stopping criteria are triggered, thus, avoiding overfitting and providing the best performance for the amplitudes.

eigenfrequencies plus two. The (17×1) MFNN is extremely accurate in the estimation of the plate eigenfrequencies, yielding $\overline{R^2} = 0.99$.

Conversely, the prediction of the amplitudes with a (17×1) MFNN topology yields $\overline{R^2} = 0.83$. To achieve a better prediction accuracy, we, thus, tune the hyperparameters of this MFNN. The procedure is implemented by varying $\mathcal{L}$ between 1 and 4 with a step of 1 and $\mathcal{M}$ between 2 and 64 with a step of 2. For each topology, we train the MFNN and evaluate the $\overline{R^2}$ on the test set. The process is repeated ten times, where the initial weights of the neurons are randomized at the beginning of each training. The final results are obtained by averaging the $\overline{R^2}$ scored by each architecture. The outcomes of the hyperparameters tuning indicate that the best MFNN for predicting the amplitudes is a (24×2) NN, yielding $\overline{R^2} = 0.94$.

Figure 4 shows the train, test, and validation losses as a function of the number of epochs obtained when (64×4) and (24×2) NNs are used to estimate the FRF amplitude, namely, the top and the bottom of the figure, respectively. It can be noted that the first network is too complex for the training data, and, thus, overfitting occurs. Indeed, the validation and test losses reach a constant high value after three epochs. Conversely, the discrepancy between the losses is acceptable for the second network, thus, avoiding overfitting and providing the best prediction for the amplitudes.

B. Application of the method

The *FRF2Params* method is employed to estimate the material parameters of a set of ten classical guitar plates of Norway spruce. The plates come in book-matched pairs. Therefore, we will denote them with respect to the pair they belong to, e.g., 1L, 1R, 2L, 2R, etc., Figure 5 shows the pictures of the samples employed in the experimental validation. Their dimensions can be found in the supplementary material.[1] It must be noted that the plates were thicknessed by the provider in an industrial sander to a nominal dimension; however, they exhibit a degree of variation inherent to the sanding process. The plates were kept in a room in a museum, which, despite not being humidity-controlled, has a rather stable humidity level of 45%. Most of the plates exhibit an irregular geometry: In particular, (i) the pairs {1R,1L} and {4R,4L} display relevant irregularities at their corners; (ii) plates 2L and 3L show moderate imperfections; and (iii) the rest do not show relevant defects.

Figure 6 shows the evolution of the optimisation cost function $\hat{L}_2$ for one of the plates and, as insets, the pairs (f_i, a_i) measured and estimated by the algorithm at initial and final steps, starting from the nominal values and Caldersmith's formulas. It can be seen here how the optimisation method is "stuck" for some time in local minima and how it eventually manages to escape and continuously improve the estimation of the material parameters. After ca. 300 iterations, the optimisation plateaus, which signals the

FIG. 5. (Color online) Pictures of the ten boards used to test the method, ordered by the pairs that were provided by the wood handler.

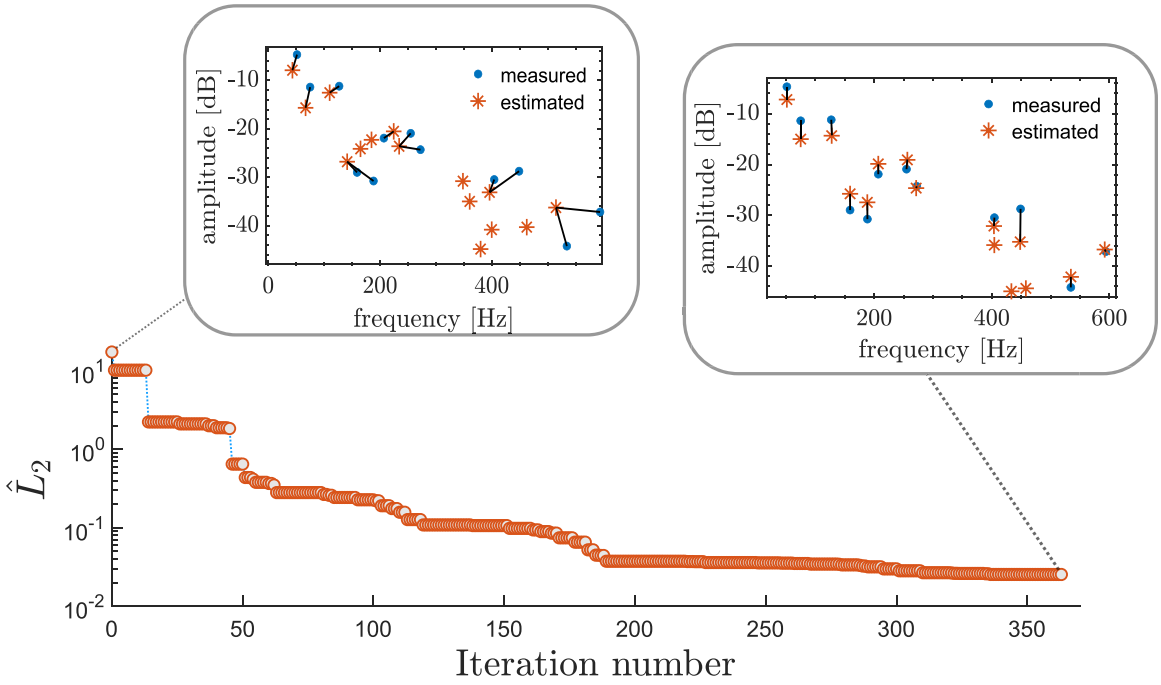

FIG. 6. (Color online) Evolution of the cost function during the optimisation process of the method. (Insets) The initial and final sets of frequency-amplitude pairs in the measured and the final optimised material parameters.

end of the optimisation process. It is possible to appreciate the great accuracy attained by the algorithm in estimating the eigenfrequencies, whereas a larger error is observable for the amplitude. This is expected, as (i) the Rayleigh damping model is known to be not accurate, despite the fact that no better alternative can be found in FEM simulation, and (ii) the amplitude is not explicitly modeled in the definition of the cost function, but only in the mode matching procedure.

The soundness of the estimated material parameters is evaluated by comparing the measured FRF to a simulated FRF, which is computed numerically using as inputs the estimates provided by *FRF2Params*. Two different metrics are computed to support the comparison. The first metric is the frequency response assurance criterion (FRAC), also known as FDAC (Heylen and Lammens, 1996; Viala *et al.*, 2021), which provides a measure of similarity between two FRFs. The FRAC yields a value in the interval $[0, 1]$, where 1 means total similarity, and 0 corresponds to no similarity. The second metric is the normalized mean squared error (NMSE) between the normalized amplitudes of the FRFs, computed as

$$\mathrm{NMSE}(\hat{y}, y) = \frac{||\hat{y} - y||_2^2}{||\hat{y}||_2^2}, \tag{14}$$

where $||\cdot||_2$ is the l_2 norm, $\hat{y}$ is the measured FRF, and y is its estimate. The NMSE is usually reported in dB.

Figure 7(a) summarizes the results in terms of NMSE (yellow bars) and FRAC (blue bars) between simulated and experimental FRFs. The best estimations are obtained for plates 2L, 2R, 5L, and 5R, which all display a great regularity in the geometry. This is expected: In this application, the NNs are not suited to predict the vibrational features of irregular plates, as they are trained on a dataset of regular plates with variable size and material parameters.

Figure 7(b) shows the normalized mobility FRF of plate 2R (solid black line) and the normalized simulated FRFs of a plate with the same geometry of plate 2R and the material parameters identified using either *FRF2Params* (dashed red line) or the theoretical Caldersmith's equations (dashed blue line). The gray areas highlight the most important differences between the measured FRF and the one obtained with Caldersmith's equations. Our method matches the measured FRF better than the theoretical prediction not only in the low modes (particularly the first), but up to the 12th peak, from which we conclude that our estimation is more accurate than the latter.

The actual values of the identified material parameters are given as supplementary material[1] to not burden the text, but it is worth noting the mean values of the ten samples for the most relevant parameters. The mean longitudinal stiffness is $\langle E_L \rangle = 11.1 \pm 1.8\,\mathrm{GPa}$, whereas the mean density for the plates is $\langle \rho \rangle = 420 \pm 24\,\mathrm{kg\,m^{-3}}$. The error associated with each plate depends on the material parameter optimised, with a rather accurate fit for the longitudinal stiffness with an error of 3%, but rather poor for the irrelevant variables: up to 60% in the estimation of the tangential stiffness for plate 5R.

To account for the geometric uncertainties associated with the thickness, we vary the density of the plates in a Gaussian manner and compute the associated best mechanical parameters for each of these realisations. This method allows us to obtain an estimate of the error associated with

https://doi.org/10.1121/10.0020559

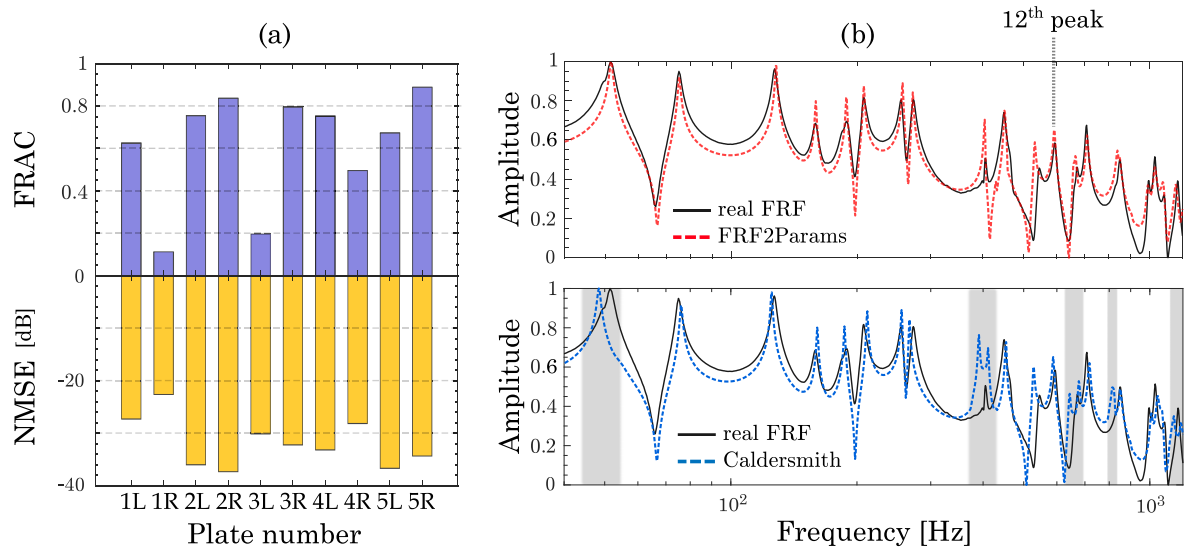

FIG. 7. (Color online) (a) FRAC (in blue) and NMSE (in yellow) between the experimental FRF of each plate and the corresponding simulated FRF using the material properties obtained with the *FRF2Params* method. (b) Normalized FRF of plate 2R (solid black line) and normalized simulated FRFs of a plate with the same geometry of plate 2R and the material parameters identified with *FRF2Params* (dashed red line) and Caldersmith's equations (dashed blue line). The gray areas highlight the discrepancy between the measured FRF and the FRF obtained with Caldersmith's equations. It is worth noting that such discrepancy is significantly reduced when *FRF2Params* is used.

density based on the sensitivity of the tools used to measure the dimensions and the weight of the plates.

VI. CONCLUSIONS

This article presents a novel data-driven technique to characterize wooden thin plates. The technique is called *FRF2Params* and allows the simultaneous estimate of plate material parameters starting from a single FRF, the geometry of the plate, and its density. Once the FRF is acquired, the method only requires the peaks of the measured FRF, without any need of further modal analysis.

The use of NNs provides us with a quick and reliable estimation of the plate vibrational properties, thus, allowing *FRF2Params* to be faster and easier to use than classical FEM updating while keeping a comparable accuracy. Thanks to these desirable features, this method can open the door to a new way of designing stringed instruments starting from the knowledge of the wood sample properties. As far as we know, such an approach is still not standard in instrument making.

An aspect that we have not thoughtfully considered is the role of the moisture content of the wood in the estimation of the mechanical parameters. When varying the moisture content, the density and all the other elastic properties vary accordingly. See Viala (2018) and references therein for an in-depth discussion. Our method works, in principle, for any moisture content but was only tested in the rather standard climatic conditions found inside a museum. Using our method in a climate-controlled room would be an excellent way to test the empirical laws that relate mechanical parameters to moisture content.

We apply the methodology to rectangular spruce plates because of their simple geometry and their wide employment in stringed instrument making. As it stands, the method only works for this particular geometry and wood species. Different materials, in particular, woods with higher density, present a different modal density in the low-frequency range and need to be dealt with in a per basis way.

The generalisation of this method to arbitrary woods and geometries poses two very distinct challenges: First, one needs to be able to predict the FRF with a NN. Increasing the number of parameters and the distribution of values of those is only a technical problem that can be solved with a combination of more data and a better architecture. Recent results in complete instruments make us confident in the feasibility of the task. Second, one needs to create minimisation algorithms that work in general for different kinds of woods and geometries, that is, for different shapes of the FRF. This is more complex since there is a qualitative change on the relation between the frequencies and amplitudes of the FRF when the material changes widely. Developing such a general method would probably involve a more complex modal fitting of the FRF, not just frequency/amplitude pairs. As such, the model will be far more dependent on the damping model used in the simulations, and a better model than Rayleigh damping will be needed (Viala *et al.*, 2021). Developing a more complete understanding of damping is probably one of the most relevant areas of wood science.

ACKNOWLEDGMENTS

The authors declare no competing interests or conflicts. The wood specimens used in this study were harvested and processed in compliance with the EU Regulation 995/2010 (European Union Timber Regulation). The wood species considered are not included in Convention on International Trade in Endangered Species of Wild Fauna and Flora

(CITES) lists. The data that support the findings of this study are openly available at https://github.com/David-Badiane/Data-driven-characterization-of-spruce-tonewood-plates.

[1]See supplementary material at https://doi/org/10.1121/10.0020559 for the measured dimensions and weight of the spruce plates used in the experiments and for the estimated mechanical parameters of the spruce plates used in the experiments.

Aldakheel, F., Satari, R., and Wriggers, P. (**2021**). "Feed-forward neural networks for failure mechanics problems," Appl. Sci. **11**(14), 6483.

Araújo, A. L., Soares, C. M., and De Freitas, M. M. (**1996**). "Characterization of material parameters of composite plate specimens using optimization and experimental vibrational data," Compos. B Eng. **27**(2), 185–191.

Badiane, D. G., Malvermi, R., Gonzalez, S., Antonacci, F., and Sarti, A. (**2022**). "On the prediction of the frequency response of a wooden plate from its mechanical parameters," in *Proceedings of ICASSP 2022—2022 IEEE International Conference on Acoustics, Speech and Signal Processing (ICASSP)*, Singapore (IEEE, New York), pp. 461–465.

Ball, P. (**2007**). "Violin makers can't pick out good wood," Nature.

Barlow, C. (**1997**). "Materials selection for musical instruments," in *Proceedings of the Institute of Acoustics UK*, Edinburgh, Vol. 19, pp. 69–78.

Beale, M. H., Hagan, M. T., and Demuth, H. B. (**1992**). *Neural Network Toolbox User's Guide* (MathWorks Inc., Natick, MA), p. 103.

Bock, F. E., Aydin, R. C., Cyron, C. J., Huber, N., Kalidindi, S. R., and Klusemann, B. (**2019**). "A review of the application of machine learning and data mining approaches in continuum materials mechanics," Front. Mater. **6**, 110.

Brauchler, A., Gonzalez, S., Vierneisel, M., Ziegler, P., Antonacci, F., Sarti, A., and Eberhard, P. (**2022a**). "Model-predicted geometry variations to compensate material variability in the design of classical guitars," Research Square.

Brauchler, A., Hose, D., Ziegler, P., Hanss, M., and Eberhard, P. (**2022b**). "Distinguishing geometrically identical instruments: Possibilistic identification of material parameters in a parametrically model order reduced finite element model of a classical guitar," J. Sound Vib. **535**, 117071.

Brauchler, A., Ziegler, P., and Eberhard, P. (**2021**). "An entirely reverse-engineered finite element model of a classical guitar in comparison with experimental data," J. Acoust. Soc. Am. **149**(6), 4450–4462.

Buksnowitz, C., Teischinger, A., Müller, U., Pahler, A., and Evans, R. (**2007**). "Resonance wood [*Picea abies* (L.) Karst.]—Evaluation and prediction of violin makers' quality-grading," J. Acoust. Soc. Am. **121**(4), 2384–2395.

Caldersmith, G. (**1984**). "Vibrations of orthotropic rectangular plates," Acta Acust. united Acust. **56**(2), 144–152.

Carlier, C., Alkadri, A., Gril, J., and Bremaud, I. (**2018**). "Revisiting the notion of 'resonance wood' choice: A decompartementalised approach from violin makers' opinion and perception to characterization of material properties variability. wooden musical instruments," in *Wooden Musical Instruments—Different Forms of Knowledge: Book of End of WoodMusICK COST Action FP1302* (Cité de la Musique, Paris, France), pp. 119–142.

Fang, Y., Lin, L., Feng, H., Lu, Z., and Emms, G. W. (**2017**). "Review of the use of air-coupled ultrasonic technologies for nondestructive testing of wood and wood products," Comput. Electron. Agric. **137**, 79–87.

Farhat, C., and Hemez, F. M. (**1993**). "Updating finite element dynamic models using an element-by-element sensitivity methodology," AIAA J. **31**(9), 1702–1711.

Fletcher, N. H., and Rossing, T. D. (**2012**). *The Physics of Musical Instruments* (Springer, New York).

Glantz, S., and Slinker, B. (**2001**). *Primer of Applied Regression and Analysis of Variance* (McGraw-Hill, New York).

Gonzalez, S., Salvi, D., Baeza, D., Antonacci, F., and Sarti, A. (**2021**). "A data-driven approach to violin making," Sci. Rep. **11**(1), 9455.

Hearmon, R. F. S. (**1948**). *The Elasticity of Wood and Plywood* (Forest Products Research, London, UK).

Heylen, W., and Lammens, S. (**1996**). "Frac: A consistent way of comparing frequency response functions," in *Proceedings of the Conference on Identification in Engineering Systems* (University of Wales, Swansea, UK), pp. 48–57.

Hornik, K., Stinchcombe, M., and White, H. (**1989**). "Multilayer feedforward networks are universal approximators," Neural Netw. **2**(5), 359–366.

Lagarias, J. C., Reeds, J. A., Wright, M. H., and Wright, P. E. (**1998**). "Convergence properties of the Nelder–Mead simplex method in low dimensions," SIAM J. Optim. **9**(1), 112–147.

Larsson, D. (**1997**). "Using modal analysis for estimation of anisotropic material constants," J. Eng. Mech. **123**, 222–229.

Lasn, K., Klauson, A., Chati, F., and Décultot, D. (**2011**). "Experimental determination of elastic constants of an orthotropic composite plate by using lamb waves," Mech. Compos. Mater. **47**(4), 435–446.

Mali, K., and Singru, P. (**2018**). "Study on the effect of the impact location and the type of hammer tip on the frequency response function (FRF) in experimental modal analysis of rectangular plates," IOP Conf. Ser. Mater. Sci. Eng. **330**, 012102.

Malvermi, R., Gonzalez, S., Antonacci, F., Sarti, A., and Corradi, R. (**2022**). "A statistical approach to violin evaluation," Appl. Sci. **12**(14), 7313.

Mclntyre, M. E., and Woodhouse, J. (**1986**). "On measuring wood properties, Part 3," J. Catgut Acoust. Soc. **45**, 14–23.

McIntyre, M., and Woodhouse, J. (**1988**). "On measuring the elastic and damping constants of orthotropic sheet materials," Acta Metall. **36**(6), 1397–1416.

Meirovitch, L. (**2001**). *Fundamentals of Vibrations* (Waveland Press, Long Grove, IL).

Moré, J. J. (**1978**). "The Levenberg–Marquardt algorithm: Implementation and theory," in *Numerical Analysis* (Springer, New York), pp. 105–116.

Mottershead, J. E., Link, M., and Friswell, M. I. (**2011**). "The sensitivity method in finite element model updating: A tutorial," Mech. Syst. Signal Process. **25**(7), 2275–2296.

Obataya, E., Ono, T., and Norimoto, M. (**2000**). "Vibrational properties of wood along the grain," J. Mater. Sci. **35**(12), 2993–3001.

Rayleigh, J. (**2013**). *The Theory of Sound* (Dover, New York), Vol. 1.

Ross, R. J. (**2010**). Wood Handbook: Wood as an Engineering Material, General Technical Report FPL-GTR-190 (U.S. Department of Agriculture Forest Service Forest Products Laboratory, Madison, WI).

Salvi, D., Gonzalez, S., Antonacci, F., and Sarti, A. (**2021**). "Parametric optimization of violin top plates using machine learning," in *"Advances in Acoustics, Noise and Vibration – 2021," Proceedings of the 27th International Congress on Sound and Vibration, ICSV 2021*, Virtual, Online, July 11–16, 2021 (Silesian University Press, Czech Republic).

Schwarz, B. J., and Richardson, M. H. (**1999**). "Experimental modal analysis," CSI Reliab. Week. **35**(1), 1–12.

Sol, H., De Visscher, J., and De Wilde, W. (**1993**). "Identification of the viscoelastic material properties of orthotropic plates using a mixed numerical/experimental technique," WIT Trans. Modell. Simul. **5**, 131–142.

Svozil, D., Kvasnicka, V., and Pospichal, J. (**1997**). "Introduction to multilayer feed-forward neural networks," Chemometr. Intell. Lab. Syst. **39**(1), 43–62.

Viala, R. (**2018**). "Towards a model-based decision support tool for stringed musical instruments making: Outil d'aide à la décision pour la facture d'instruments de musique à cordes," Ph.D. thesis, Université Bourgogne Franche-Comté, Bourgogne Franche-Comté, France.

Viala, R., Pérez, M. A., Placet, V., Manjón, A., Foltête, E., and Cogan, S. (**2021**). "Towards model-based approaches for musical instruments making: Validation of the model of a Spanish guitar soundboard and characterization features proposal," Appl. Acoust. **172**, 107591.

Viala, R., Placet, V., and Cogan, S. (**2018**). "Identification of the anisotropic elastic and damping properties of complex shape composite parts using an inverse method based on finite element model updating and 3D velocity fields measurements (FEMU-3DVF): Application to bio-based composite violin soundboards," Compos. A Appl. Sci. Manuf. **106**, 91–103.

Viala, R., Placet, V., and Cogan, S. (**2020**). "Simultaneous non-destructive identification of multiple elastic and damping properties of spruce tonewood to improve grading," J. Cult. Herit. **42**, 108–116.

Wegst, U. G. (**2006**). "Wood for sound," Am. J. Bot. **93**(10), 1439–1448.

Yoshikawa, S. (**2007**). "Acoustical classification of woods for string instruments," J. Acoust. Soc. Am. **122**(1), 568–573.

Zhou, J., Chui, Y. H., Gong, M., and Hu, L. (**2017**). "Comparative study on measurement of elastic constants of wood-based panels using modal testing: Choice of boundary conditions and calculation methods," J. Wood Sci. **63**(5), 523–538.